Direct Conversion of CO_2 into Alcohols Using Cu-Based Zeolite Catalysts

Iltsiou, Dimitra; Mielby, Jerrik; Kegnæs, Søren

Published in:
ChemPlusChem

Link to article, DOI:
10.1002/cplu.202300313

Publication date:
2024

Document Version
Publisher's PDF, also known as Version of record

ChemPlusChem

Research Article
doi.org/10.1002/cplu.202300313

Chemistry Europe
European Chemical Societies Publishing

www.chempluschem.org

Special Collection

Direct Conversion of CO_2 into Alcohols Using Cu-Based Zeolite Catalysts

Dimitra Iltsiou,[a] Jerrik Mielby,*[a] and Søren Kegnæs*[a]

The direct hydrogenation of CO_2 into alcohols is an attractive but challenging catalytic reaction. Herein, it was shown that Cu nanoparticles supported on MFI and BEA zeolites have high catalytic activity and selectivity for converting CO_2 into ethanol and isopropanol. Furthermore, we investigated the effect of introducing mesopores via carbon templating and encapsulating the Cu nanoparticles via subsequent recrystallization. All the catalysts were characterized by N_2 physisorption, XRD, SEM, TEM, NH_3 TPD, XPS, and XRF, before we tested them in a high-pressure water-filled autoclave with a constant partial pressure of CO_2 (1 MPa) and an increasing partial pressure of H_2 (3–5 MPa). In general, the mesoporous zeolite catalysts resulted in a higher CO_2 conversion and selectivity toward ethanol than their non-mesoporous equivalents, while the recrystallized catalyst with encapsulated Cu nanoparticles had a higher selectivity towards isopropanol. For example, Cu@m-S1 showed the highest isopropanol productivity among the recrystallized mesoporous zeolites, corresponding to 20.51 mmol g^{-1} h^{-1} under the given reaction conditions. These findings highlight the importance of mesopores in zeolite catalysts for CO_2 hydrogenation to alcohols and point a new direction for further research and development.

Introduction

New technologies for carbon capture, utilization, and storage are critically needed to limit our emissions of harmful greenhouse gasses.[1,2] The production of green H_2, using renewable energy sources, has gained significant attention as a potential pathway for catalytic hydrogenation of CO_2 to produce high-value chemicals, including olefins, gasoline, aromatics, and alcohols, including methanol.[3–8] Now, attention is being directed towards the formation of higher alcohols (C_{2+}), although the selective C–C coupling becomes increasingly challenging, as reported by previous studies.[6,9] The direct conversion of CO_2 into ethanol has been the focus of extensive research due to its potential as a hydrogen carrier, fuel additive, and a building block for producing other high-value chemicals.[14,15] Unfortunately, the yield of ethanol, produced directly from CO_2, is typically low.[16–19] In general, the direct synthesis of ethanol and higher alcohols from CO_2 is limited by the challenging C–C coupling among different species, such as CH_xO and CH_x (x = 0–3).[20]

A wide range of catalysts (shown in Table S1) has been used to directly convert CO_2 into alcohols. The synthesis of C_{2+} oxygenates is usually carried out using Co-,[21–23] Mo-,[24,25] Rh-,[26–28] and Cu-[29,30] based catalysts. Cu-based catalysts have been extensively used to hydrogenate CO and CO_2 into oxygenates from syngas, because of their high selectivity and activity, which are highly dependent on the support and/or promoters.[31–33] Recently, zeolites have also gained attention as potential supports for CO_2 hydrogenation.[26,29] Among the many remarkable properties, zeolites can have Brønsted and Lewis acidity, both cations, complexes, and metal nanoparticles.[34–41] For example, the encapsulation of metal nanoparticles inside the microporous zeolites can increase the dispersion, stabilize the nanoparticles against sintering, and introduce shape selectivity by limiting the diffusion of large and bulky reactants, intermediates, and/or products through the zeolite.[40,42–46] If the limited diffusion becomes a disadvantage, it is also possible to prevent some of the mass transfer limitations by introducing secondary mesopores in the microporous zeolite.[42,47] The development of mesoporous zeolites is an attractive solution, as mesoporous zeolites have many potential applications in catalysis, adsorption, and separation processes.[48–52] The diameter of mesopores is between 2 and 50 nm, which is larger than the typical micropores found in zeolites.[53] This increases the diffusivity and allows larger molecules to access the active sites inside the zeolite, which increases the catalytic activity.[53–58] There are several efficient methods to introduce mesopores in zeolites, including template-assisted and post-synthesis treatments. In carbon-templating, the zeolite gel is typically mixed with a carbon template that is then subjected to a hydrothermal synthesis.[59–61] When the zeolite has crystallized around the template, the carbon is simply removed by calcination in air. This approach has previously been used for a number of zeolites, including the MFI zeolites, ZSM-5, and Silicalite-1 (S1), and the BEA zeolite (Beta),[59–61] leading to higher activity in a

[a] D. Iltsiou, Dr. J. Mielby, Prof. S. Kegnæs
Department of Chemistry,
Technical University of Denmark
Kemitorvet 207, 2800 Kgs. Lyngby (Denmark)
E-mail: jjmie@kemi.dtu.dk
skk@kemi.dtu.dk

Supporting information for this article is available on the WWW under https://doi.org/10.1002/cplu.202300313

Special Collection Part of a Special Collection on Green Chemistry

variety of catalytic applications, including cracking, hydrocracking, and alkylation.[61–67] Additionally, the mesoporous structure makes the active sites more accessible, resulting in higher selectivity and longer catalyst lifetimes.[60,68]

In this work, we studied the direct hydrogenation of CO_2 into alcohols and tested the catalytic effect of introducing mesopores in ZSM-5, S1, and Beta zeolites containing Cu nanoparticles. First, we synthesized the mesoporous zeolites by carbon templating with carbon black (BP2000), before we impregnated the mesoporous zeolites (m-zeolites) with 1 wt% Cu by incipient wetness impregnation (Cu/m-zeolites). Furthermore, we also subjected the Cu/m-zeolites to a recrystallization step to synthesize the catalysts Cu@m-zeolites with encapsulated nanoparticles (see Figure 1). Our study confirms that polar solvents, such as water, are essential to increase the yield of alcohols.[70,71] Furthermore, we show that the introduction of mesopores and high partial pressures of H_2 favor the formation of isopropanol, while methanol, ethanol, and CO are the main products at lower pressures in zeolites without mesopores.

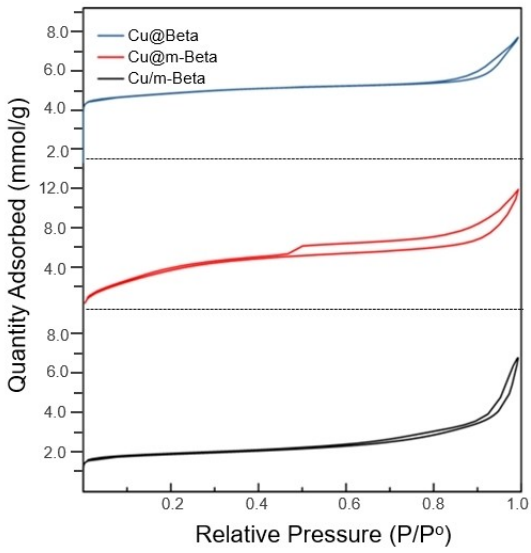

Figure 2. N_2 physisorption isotherms of the Cu-containing Beta zeolite catalysts.

Results and Discussion

Structural and Chemical Characterization Results

Table 1 compiles the results of the N_2 physisorption of the Cu-containing zeolite catalysts and XRF, and Figure 2 shows the N_2 physisorption isotherms of the Cu-containing Beta catalysts. In general, the physisorption data show how the introduction of mesopores results in a clear increase in the specific surface area and total pore volume. Table 1 illustrates that the external surface area of the recrystallized mesoporous catalysts surpasses that of the Cu-containing non-mesoporous catalysts, albeit by a slight margin. However, in the case of Cu-containing mesoporous catalysts, the external surface area is much more significant. Furthermore, the data show that the recrystallization did not significantly affect the surface area and micropore volume, although the total pore volume decreased as the Cu/m-zeolites were converted into Cu@m-zeolites.

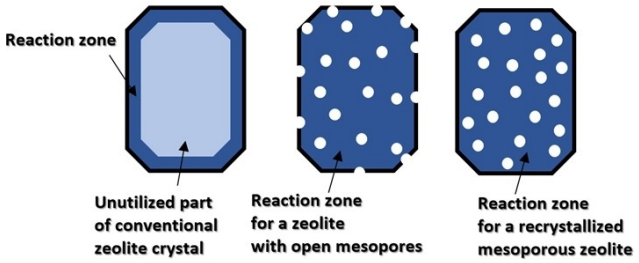

Figure 1. Schematic illustration of the reaction zones in conventional zeolites and zeolites with intracrystalline mesopores.

The physisorption isotherms in Figure 2 reveal more details about the morphology of the recrystallized Beta zeolites; see Figure S3 for the other materials. As expected, all the Cu-containing zeolites have a significant adsorption of N_2 at the low relative pressures ($P/P^o < 0.01$) due to the presence of micropores. For the Cu/m-zeolites, a significant hysteresis loop at $P/P^o = 0.50$ indicates the presence of a broad distribution of

Table 1. N_2 Physisorption and XRF results for the Cu-containing zeolites.

Sample	V_{micro} (cm^3/g)[a]	V_{total} (cm^3/g)[b]	Surface area (m^2/g)[c]	External surface area (m^2/g)[d]	Si/Al
Cu/S1	0.11	0.24	385	128	
Cu/m-S1	0.13	0.35	420	140	
Cu@m-S1	0.13	0.32	409	133	
Cu/ZSM-5	0.07	0.22	327	112	30
Cu/m-ZSM-5	0.12	0.32	395	134	29
Cu@m-ZSM-5	0.12	0.29	377	119	37
Cu/Beta	0.08	0.23	410	145	32
Cu/m-Beta	0.14	0.33	507	169	19
Cu@m-Beta	0.12	0.31	490	150	26

[a] Estimated by the t-plot method, [b] estimated from a single point adsorption of 0.95 relative pressure, [c] estimated by the BET method, [d] estimated by XRF.

large mesopores.[37,42] According to the IUPAC classification, the physisorption isotherms of the mesoporous materials is a type IV with an H1 hysteresis loop. For the Cu@m-zeolites, the hysteresis loops are closing at P/P° = 0.45, which corresponds to a type IV histogram with a H2a porosity, indicating that the Cu@m-zeolites contain a system of internal voids and mesopores.[37,42] In the isotherm, due to the so-called tensile strength effect (TSE), the hysteresis loop has a distinctive forced closure at P/P = 0.45.[69]

Figure 3 shows the diffractograms of the mesoporous Cu-containing Beta, ZSM-5, and S1 catalysts, respectively. In general, the diffractograms did not reveal any significant differences among the Cu/zeolites, Cu/m-zeolites, and Cu@m-zeolites.

The absence of a broad background indicates a high crystallinity. The absence of peaks from CuO at 35.3° and 39.8°, shows that the size of Cu nanoparticles is too small to be detected by XRD. Figure S2 compiles the diffractograms of all the Cu-containing zeolite catalysts that were tested in this study.

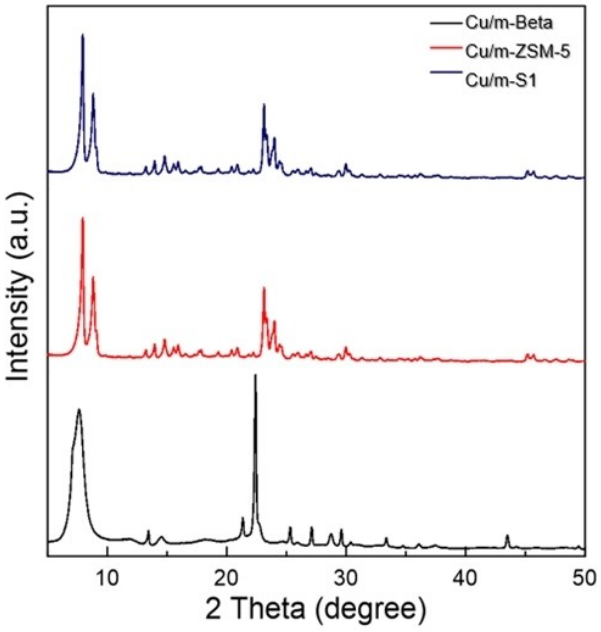

Figure 3. XRD patterns of the Cu/m-zeolite catalysts encapsulated with 1 wt % of Cu.

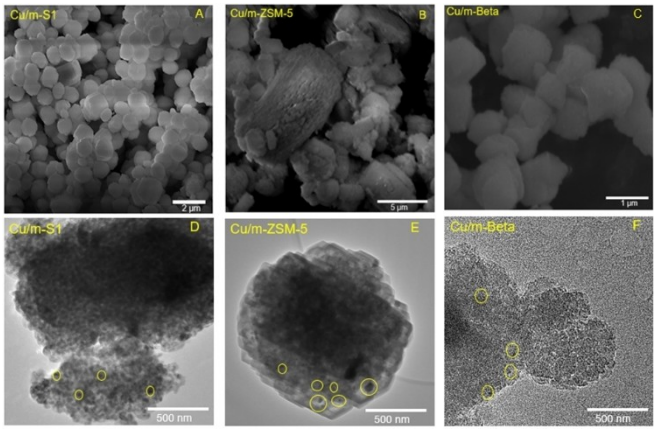

Figure 4. SEM pictures of A) Cu/m-S1, B) Cu/m-ZSM-5, C) Cu/m-Beta, and TEM pictures of D) Cu/m-S1, E) Cu/m-ZSM-5, D) Cu/m-Beta.

Figure 4 shows the TEM pictures of A) Cu/m-S1, B) Cu/m-ZSM-5, C) Cu/m-Beta, and SEM pictures of D) Cu/m-S1, E) Cu/m-ZSM-5, D) Cu/m-Beta. Figures S4–S14 show the SEM, EDX, and TEM pictures of all the Cu-containing zeolite catalysts, respectively. According to the SEM images, the size of the zeolite crystals at the recrystallized Cu@m-zeolites is ranging from 1 μm to 5 μm, the same as for Cu/m-zeolites. This demonstrates that, during recrystallization, the zeolite precursors crystallize on the surface of the mesoporous Cu/m-zeolites that act as seed crystals.

In the SEM images (Figure 4D–F), the open pores appear as the rough surface features of the mesoporous catalysts.[42] For comparison, the surface of the non-mesoporous zeolites shows smooth, well-defined crystal facets (Figures S4A, S8A, and S11A). Figures S4B, S8B, and S11B show how the steam-assisted recrystallization has changed the surface of the Cu/m-zeolites and transformed the open porosity into small compartments. The zeolite shell thickness is around the range of 20–40 nm. Figure S15 shows the XPS analysis for the Cu 2p orbitals in the Cu-containing Beta catalysts. We assigned the four peaks at 935 eV, 940–945 eV, 955 eV, and 963 eV, to the Cu $2p_{3/2}$, Cu $2p_{3/2}$ (strong satellite Cu^{2+} signal), Cu $2p_{1/2}$, Cu $2p_{1/2}$ (strong satellite Cu^{2+} signal) of CuO, respectively. In Figures S15A and S15B, for the Cu/Beta and Cu/m-Beta, it is also possible to observe the Cu $2p_{3/2}$ peaks, which indicate the presence of Cu nanoparticles on the outer surface of the Cu/Beta and Cu/m-Beta. However, the absence of these peaks in S15B, shows that the Cu is located inside the zeolite. The differences in the signal intensities indicate that there is more Cu present on the surface of Cu/Beta than on Cu/m-Beta, maybe because of the larger pores of the mesoporous BEA framework. Table S2 shows the results of the XRF analysis regarding the Cu loading of all catalysts. As expected, the Cu loading of the Cu@m-zeolites is slightly lower than the Cu/m-zeolite catalysts because of the added zeolite precursors. The NH_3-TPD analysis in Table 2 and Figure S16 shows that the distribution of strong and weak acid sites were similar for all Cu-containing MFI zeolites. The Cu-containing Beta zeolites were considerably more acidic than Cu-containing MFI zeolites, and they showed two distinct peaks with high intensity at the strong acid site region at around 350–400 °C (Figure S16C).

Catalytic tests

The influence of the solvent was first investigated in CO_2 hydrogenation reactions with the catalyst Cu@m-Beta. Table S3 shows the results from the catalytic tests with different solvents, including water, cyclohexane, toluene, tetrahydrofuran (THF) and N,N-Dimethylformamide (DMF). The results show that the solvent has a significant impact on reaction and that water resulted in the highest yield of ethanol reaching a productivity of 50.3 $mmol\,g^{-1}\,h^{-1}$. In comparison, DMF only produced

Table 2. Distribution of strong and weak acid sites as estimated by NH_3-TPD.

Catalyst	Weak acid sites[a] (mmol/g)	Strong acid sites[b] (mmol/g)
Cu@m-Beta	0.429	0.200
		0.231
Cu/m-Beta	0.436	0.207
		0.323
Cu/Beta	0.417	0.210
		0.299
Cu@m-ZSM-5	0.038	0.119
Cu/m-ZSM-5	0.059	0.121
Cu/ZSM-5	0.037	0.107
Cu@m-S1	0.069	0.156
Cu/m-S1	0.081	0.163
Cu/S1	0.079	0.178

[a] Weak acid sites as estimated by NH_3-TPD when NH_3 desorbed at 180 °C–280 °C,[b] Strong acid sites as estimated by NH_3-TPD when NH_3 desorbed at 280 °C–600 °C.

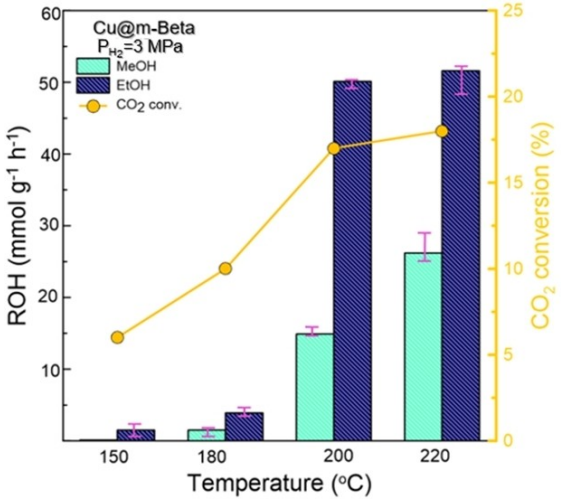

Figure 5. Productivity for methanol and ethanol for Cu@m-Beta in different temperatures.

0.13 mmol g^{-1} h^{-1}, while cyclohexane, toluene, and tetrahydrofuran produced no ethanol. Water's improved performance is due to its highly polar character, which allows it to effectively solvate the reactants and facilitate efficient mass transfer, resulting in higher reaction rates.[70–72] We note that, the CO_2 solubility is significantly higher in water than in DMF and THF or the nonpolar solvents tested. This is important for CO_2 hydrogenation reactions since CO_2 is the main reactant and must be dissolved in the solvent in order to react with H_2. Additionally, THF is lacking labile hydrogen atoms, which are essential to facilitate proton transfer for alcohol synthesis. In contrast, water's strong hydrogen bonding capability can improve catalyst stability and promote the formation of desired products such as ethanol.[72] Cyclohexane and toluene are nonpolar solvents that lack the ability to effectively dissolve and interact with ionic and polar compounds, which are crucial in the CO_2 hydrogenation process. According to Graciani *et al.* and Wang *et al.*, water plays a crucial role in catalyzing the conversion of CO_2 into valuable chemicals like ethanol and methanol, respectively.[70,71] It enhances the surface coverages of key intermediates, influences product selectivity, and facilitates essential reaction steps, ultimately improving reaction kinetics and overall efficiency in these catalytic systems.

To examine the impact of temperature and reaction time, the catalyst Cu@m-Beta was chosen for its high yield and selectivity to ethanol, at a partial H_2 pressure 3 MPa. Figure 5 shows how the production of ethanol and methanol increases steadily as we increase the temperature from 150 °C to 220 °C. Unfortunately, the higher temperatures also increased the formation of methanol, reducing the ethanol selectivity to 55% at 220 °C. Consequently, we chose 200 °C as the optimum temperature for the reaction. Figure S17 shows the effect of the reaction time on the yield and selectivity towards the production of ethanol and methanol. Although the initial yield was quite low (2.18 mmol g^{-1} h^{-1}), rapidly increased to 50.13 mmol g^{-1} h^{-1} in the first hour and then settled at around 14.95 mmol g^{-1} h^{-1} for methanol. These results suggest that the formation of methanol may be a critical intermediate for the formation of ethanol. To validate this hypothesis, we used the Cu@m-Beta catalyst at 200 °C under a partial H_2 pressure of 3 MPa. In the autoclave, we introduced 5 ml of water and 0.15 µl of methanol-d4. We aimed to observe through D NMR, if ethanol-d6 would be produced. Figure S18A–B displays the ^{1}H NMR and D NMR spectra, revealing the presence of ethanol, methanol, and d-6 ethanol under the specified conditions. Notably, distinct peaks corresponding to methanol-d4 (at 3.34 ppm) and ethanol-d6 (at 1.20 and 3.66 ppm) are evident, along with OD signals around 4.8 ppm. These compelling data supports our claim that methanol serves as an intermediate product, subsequently transforming into ethanol. Additionally, Figure S19 indicates that while not all methanol-d4 was consumed for ethanol-d6 production within the initial 5-hour period, over 18 hours, complete consumption of methanol-d4 was achieved, resulting in a product mixture containing 0.0018 mmol of ethanol-d6.

All the Cu-containing zeolites produced ethanol, methanol and CO at 200 °C under 1 MPa CO_2 and 3 MPa H_2 in water (Figure 6A and Table S4). However, by increasing the partial H_2 pressure of 4 and 5 MPa, we also formed isopropanol (6B, S17, and Table S5 and S6). When comparing the BEA and MFI frameworks, we found that the Cu-containing Beta zeolites produced ethanol and methanol in higher yields, while the Cu-containing MFI zeolites produced more isopropanol.

When the partial H_2 pressure was 3 MPa, Cu/ZSM-5 and Cu/S1 showed the lowest conversions of CO_2, 7% and 9%, respectively.

The conversion is slightly increased in higher hydrogen partial pressures (4 MPa and 5 MPa), but it differs from the mesoporous samples, in which it reaches at 10% for the Cu/m-ZSM-5 and 15% for Cu/m-S1.

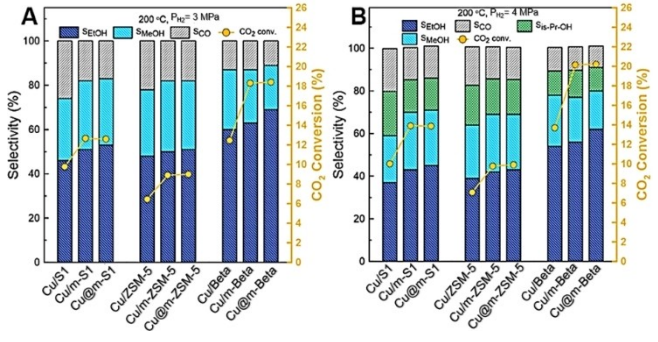

Figure 6. CO_2 conversion and product selectivity for all the Cu-containing zeolites under 200 °C and partial H_2 pressure of A) 3 MPa and B) 4 MPa.

At a partial pressure of 4 MPa H_2, the Cu@m-S1 catalyst produced up to 28.60 mmol g^{-1} h^{-1} of ethanol, with a selectivity of around 52 %. Cu/ZSM-5 only resulted in ethanol selectivity of around 44 %, although we note that this is higher than other catalysts tested under the same conditions.[30,32,68] Cu/ZSM-5 produced less ethanol and methanol than Cu/S1 under all reaction conditions tested, which showed that the presence of aluminum is not prerequisite for achieving a high catalytic activity. Under a partial pressure of 5 MPa H_2, Cu@m-S1 resulted in isopropanol productivity of 17.79 mmol g^{-1} h^{-1}, followed by Cu/m-S1 and Cu/S1, which produced 14.83 mmol g^{-1} h^{-1} and 12.09 mmol g^{-1} h^{-1}, respectively. Recently, Zhang *et al.* showed that Rh nanoparticles encapsulated in S1 were active for the direct conversion of CO_2 and H_2 into alcohols in a high pressure fixed bed reactor at 250 °C and a total pressure of 5 MPa. The authors highlighted that the presence of Na^+ was crucial for achieving high ethanol selectivity and low CH_4 production. This is attributed to Na^+ inducing the coexistence of Rh^0 and Rh^+ species.[28] The highest selectivity to ethanol was 24 %, the CO_2 conversion 10 %, and the greatest ethanol space-time yield was 72 mmol g^{-1} h^{-1}. The Cu-containing ZSM-5 and S1 zeolites have the same pore topology, although the ZSM-5 contains pentavalent Al atoms that may be charge-compensated by Cu or Na ions. According to Table 1, the Cu-containing S1 catalysts have higher surface area and pore volume than the Cu-containing ZSM-5 catalysts. Therefore, when comparing the S1 and ZSM-5 zeolites, mesoporosity influenced the quantity of alcohols generated, rather than the presence of Al in the zeolite. The synthesis protocol clearly confirms the presence of Na^+ ions in the ZSM-5 zeolite. However, the similar selectivities to alcohols observed for the Cu-based ZSM-5 and S1 catalysts suggest that the presence of Na^+ did not affect the selectivity of these alcohols. Nevertheless, when employing the H–Cu/ZSM-5 catalyst without any Na^+ ions, the primary products were CH_4 and CO (see Table S4). Methanol showed a low selectivity of 2 %, underscoring the pivotal role of alkali metals in driving the reaction towards higher alcohol production. The inclusion of Cu within the zeolite framework emerges as a critical factor for ethanol production, as demonstrated in comparative studies where Cu/SiO_2 exhibited significantly lower CO_2 conversion and lacked ethanol production.[29,73] In accordance with this, Wang *et al.* excluded Cu/SiO_2 from consideration for ethanol production due to its inherent stability issues, which present a hurdle for broad industrial implementation.[73] They reported an impressively stable Cu/SiO_2 nanocatalyst, showcasing noteworthy CO_2 conversion towards methanol. Cu@m-Beta resulted in the highest conversion (17 %) and ethanol selectivity (68 %) under 3 MPa, reaching a productivity of 50.13 mmol g^{-1} h^{-1}. To the best of our knowledge, these results surpasses previous results from similar autoclave experiments.[21–32] Comparing the different Cu-containing zeolite catalysts, the conventional zeolites resulted in significant amounts of CO, which indicated that the introduction of mesopores favors the production of alcohols. The lower selectivity to isopropanol observed in Cu-containing Beta zeolites may be attributed to the slightly lower Si/Al ratio (Si/Al = 34) compared to ZSM-5 zeolites (Si/Al = 48), or to it's larger pores that appear to favor the CO_2 conversion. At a partial pressure of 5 MPa H_2, Cu@m-Beta resulted in 20.62 mmol g^{-1} h^{-1} of methanol and 60.65 mmol g^{-1} h^{-1} of ethanol, which was the highest total productivity of alcohols among all the catalysts and reaction conditions (Table S6, Figure S20). These results highlight the potential of Cu-containing zeolites, specifically Cu@m-Beta, as highly efficient catalysts for the direct hydrogenation of CO_2 into alcohols.

Post-reaction characterization was carried out to investigate any structural changes of the catalyst Cu@m-Beta at two distinct time intervals: after 5 hours and 18 hours of reaction. The results, displayed in Figure 21A–C and Figure 21D–F, feature TEM images from the respective time points. Interestingly, it was observed that the porosity of the Cu@m-Beta catalyst remained largely intact throughout the reaction duration. However, we observed the presence of Cu nanoparticles in the edges of the zeolite. The mesoporous zeolite Beta proves to be an efficient support for stabilizing Cu nanoparticles, enabling sustained ethanol production over an extended 18-hour period.

Future research could focus on optimizing the Si/Al ratio and exploring the influence of various reaction parameters to enhance the catalytic performance further. Ding *et al.* reported the synthesis of Beta zeolite encapsulated with 8 wt% Cu nanoparticles (denoted as Cu@Na-Beta) with size of 2 to 5 nm.[29] Using the Cu@Na-Beta in a fixed bed reactor at 300 °C and 2.1 MPa, resulted in 8.63 mmol g^{-1} h^{-1} ethanol. Methanol and CH_4 were not reported and the selectivity to ethanol was around 70 %, while the selectivity to CO was around 30 %. The conversion of CO_2 was around 7 %.[29] The authors proposed that the Cu nanoparticles dispersed and became integrated into the pores of the Na-Beta support, thereby enhancing the activity and yield of the catalyst. Furthermore, they claimed that the presence of Na-Beta encapsulating the Cu nanoparticles inhibits the formation of undesired byproducts. XANES spectra analysis confirmed the reduction of CuO to metallic Cu, which served as the active species.[29] For the catalysts Cu@m-zeolites, the inclusion of auxiliary mesopores significantly impacted product selectivity, particularly for ethanol production. These mesopores facilitated reactant access to Cu active sites, enhancing the interaction and driving specific chemical reactions leading to ethanol formation. This observation was

consistent with Ding *et al.*'s study, which employed alkali etching to encapsulate active copper nanoparticles within zeolite mesopores. This strategy stabilized the nanoparticles in mesopores, enabling CO_2 bonding with adsorbed methyl groups, forming the crucial intermediate CH_3COO , ultimately yielding ethanol through hydrogenation. This confinement approach profoundly influenced Cu nanoparticle morphology, playing a crucial role in the CO_2-to-ethanol conversion process. Hence, in the case of both the Cu@Na-Beta and our Cu-containing zeolite catalysts, the pores within the zeolite structure stabilized the metal nanoparticles and potentially impeded the formation of undesired byproducts, thereby enhancing the selectivity towards ethanol.

Conclusions

We synthesized Cu-containing BEA and MFI zeolites and their mesoporous equivalents by carbon templating. The Cu content was around 1 wt%, and the mean size of the Cu nanoparticles was around 2 nm. The direct hydrogenation of CO_2 into methanol, ethanol, and isopropanol was achieved in water-filled autoclaves. The introduction of mesopores in the zeolite increases both the conversion and the selectivity. The large pore Cu-containing Beta zeolite was more effective for the production of ethanol, while the non-mesoporous catalysts produced more CO. At high partial pressure of H_2 (4 MPa and 5 MPa), all the Cu-containing zeolites also resulted in the formation of isopropanol. The production of isopropanol was favored by the introduction of mesopores. The recrystallized catalyst with encapsulated Cu nanoparticles, Cu@m-S1, resulted in a productivity of up to 20.51 mmol g^{-1} h^{-1} of isopropanol. In conclusion, the utilization of mesoporous Cu-based zeolites has proven to be a significant advancement in enhancing CO_2 conversion when compared to their non-mesoporous Cu-based equivalents. Specifically, Cu/m-Beta stands out as a remarkable catalyst. At a partial pressure of H_2 of 3 MPa, it achieved a notable CO_2 conversion rate of 18%. With a slight increase to 4 MPa, the conversion rate further improved to an impressive 20%. Pushing the boundaries even higher, at 5 MPa, Cu/m-Beta exhibited its remarkable potential by achieving a remarkable CO_2 conversion rate of 22%. These results underscore the effectiveness of mesoporous Cu-based zeolites, in addressing the challenges associated with CO_2 conversion towards alcohol.

Experimental Section

Materials

All chemicals were used for the syntheses without further purification: NaOH pellets (99%, VWR chemicals), tetrapropylammonium hydroxide (TPAOH, 1 M in water, Sigma Aldrich) tetraethylammonium hydroxide (TEAOH, 35 wt%, Sigma Aldrich), fumed silica (SiO_2, Davisil Grade 62, pore size 160 Å), sodium aluminate ($NaAlO_2$, 54 wt% Al_2O_3 and 41 wt% Na_2O, Sigma Aldrich), $Al_2(SO_4)_3 \cdot 18H_2O$ (aluminum sulfate octadecahydrate, Sigma Aldrich), tetraethyl orthosilicate (TEOS, 99% Sigma Aldrich), copper (II) nitrate hydrate ($Cu(NO_3)_2 \cdot xH_2O$, 99.999%), BP2000 black pearls (average diameter 12 nm, Cabot Corporation), HF (40 wt%, Sigma Aldrich).

Synthesis of the Cu-containing zeolites

Exemplified for the Beta zeolite, the synthesis of the mesoporous Beta was done according to the reported procedure of Egebald *et al.*[67] BP2000 was left to dry overnight at 80 °C. TEOS (3.7 ml), TEAOH (7.9 ml), H_2O (0.55 ml) and $NaAlO_2$ (350 mg) were mixed and stirred for 10 min in a Teflon beaker. Once dried, 2 g BP2000 were added to the clear solution and the mixture was stirred in room temperature for 6 hours, until the evaporation of ethanol formed by the hydrolysis of TEOS. Then, 0.95 g of HF were added to the mixture, which resulted directly to the formation of a thick gel. The carbon-gel composite was placed in Teflon lined stainless steel autoclave and left to crystallize at 170 °C for 3 days. The resulting product (denoted as m-Beta) was isolated by centrifugation, then washed until neutral pH and calcined at 550 °C for 20 hours.

The m-Beta was dried at 60 °C in vacuo overnight and was impregnated with an aqueous solution corresponding to 1 wt% Cu. After the incipient wetness impregnation, the solid was dried overnight, and then calcined at 550 °C for 5 hours with a temperature ramp of 3 hours, and reduced under a flow of 5 vol.% H_2/N_2 at 350 °C for 2 hours with a temperature ramp of 5 °C/min to yield the material denoted as Cu/m-Beta.

The recrystallization of Cu/m-Beta was done by mixing the Cu-containing zeolite with 3.12 ml TEAOH, 1 ml deionized H_2O, 540 mg fumed silica and 175 mg of $NaAlO_2$. The solution stirred for 4 hours and then introduced to a Teflon lined stainless steel autoclave. The autoclave was placed in an oven at 170 °C for 3 days. Recrystallized Cu/m-Beta (Cu@m-Beta) was obtained after the powder was separated by centrifugation, washed to neutral pH, and calcined at 550 °C for 5 hours.

Catalyst Characterization

X-ray powder diffraction (XRPD) was carried out by using a HUBER G670 Gionier camera, operated in transmission mode by using Cu–Ka radiation. The powders were measured with 0.005° steps for 1 hour.

The N_2 physisorption analysis was performed with a Micromeritics 3Flex instrument. Prior to the measurements, the catalysts were degassed at 400 °C overnight under vacuum. The Brunauer-Emmett-Teller (BET) method was used to estimate the specific surface area. The pore volume of the materials was estimated by a single point adsorption at 0.95 relative pressure. The t-plot method was used to calculate the micropore volume and the Barrett-Joyner-Halenda (BJH) method on the desorption brand was used for the pore size distribution.

Transmission electron microscopy (TEM) was performed on the calcined Cu-containing zeolites on a FEI Tecnai T20 G2 microscope with 200 kV acceleration voltage.

X-ray photoelectron spectroscopy (XPS) analysis was conducted on a ThermoFischer Scientific K-Alpha™ with a monochromated Al Kα X-ray source. The elemental spectra were measured with a pass energy of 50 eV and step size of 0.1 eV, at an operating vacuum of about $2 \cdot 10^{-7}$ mbar.

Scanning electron microscopy (SEM) was done on a Quanta 200 ESEM FEG operated at 20 kV. The samples were loaded on carbon tape and coated with gold for 60 seconds at 20 nA current in argon atmosphere.

NH_3 Temperature programmed desorption (NH_3 TPD) was performed on a micromeritics ASAP 2020. Initially, the samples were heated to 500 °C in flow of N_2. The temperature was then decreased at 150 °C and subsequently, the gas was changed to an NH_3 flow for 30 minutes, before the catalyst was flushed with N_2 for 3 hours to remove the physically adsorbed NH_3.

X-ray Fluorescence (XRF) was done in a PANanalytical Epsilon 3X. Prior to the measurement, the powders (250 mg) were mixed with the non-wetting agent LiBr (0.60 g) and Lithium Borate Flux (10.5 g). A Claisse LaNEO FLuxer was used to melt and mix the sample at 1050 °C before it was poured into a Pt mold to create a glass discs for the XRF measurements.

Catalytic reaction

The catalytic reactions were performed in 75 ml stainless-steel Berghof BR-100 autoclaves. In an exemplified synthesis, 5 mg of catalyst and 5 ml H_2O were poured into the Teflon insert together with a magnetic stirring bar. Then the autoclave was closed and flushed with N_2 three times before it was filled with 1 MPa of CO_2 and then H_2 until a total pressure of 4, 5, or 6 MPa (making the partial pressure of H_2 3, 4 and 5 MPa, respectively). The autoclave reactor was then heated to 200 °C with a heating ramp of 1 hour, and kept at 200 °C for 5 hours. After cooling, a gas sample was injected in an Agilent 7890A GC-FID-MS system equipped with a CP-Chirasil-DEx CB column to estimate the CO_2 conversion and the CO selectivity. ^{1}H NMR analysis of the liquid products was then performed to identify and quantify the alcohols produced under the reaction conditions by using deuterium oxide (D_2O) as a solvent. Figure S1 show typical ^{1}H NMR spectra of the reaction mixtures using Cu/m-Beta at 200 °C under different pressures.

Supporting Information

The supporting information provides a detailed list of catalysts used in the CO2 hydrogenation to ethanol, including synthesis methods for the Cu-containing ZSM-5 and S1 catalysts. Furthermore, it includes the characteristic ^{1}H NMR spectra illustrating the reaction results at different pressures (at 200 °C), XRD patterns, SEM, TEM, and EDS images, XPS spectra, XRF results, and NH_3-TPD spectra for all the catalysts. In addition, the supporting information include tables presenting the reaction results and figures showing the CO_2 conversion and product selectivity for all Cu-containing zeolites under conditions of 200 °C and a partial H_2 pressure of 5 MPa. Moreover, it provides information on the production of alcohols and selectivity versus the time of reaction.

Acknowledgements

This work was supported by Independent Research Fund Denmark (grant no. 6111-00237 and 0217-00146B), Haldor Topsøe A/S, Villum fonden (Grant No. 13158) and the European Union's Horizon 2020 research and innovation program under grant agreement No. 872102. The authors gratefully acknowledge the Department of Chemistry, Technical University of Denmark (DTU) for the support of the project.

Conflict of Interests

The authors declare no conflict of interest.

Data Availability Statement

The data that support the findings of this study are available from the corresponding author upon reasonable request.

Keywords: ethanol · hydrogenation · porosity · zeolites

[1] E. S. Sanz-Perez, C. R. Murdock, S. A. Didas, C. W. Jones, *Chem. Rev.* **2016**, *116*, 11840–11876.
[2] G. A. Olah, G. S. Prakash, A. Goeppert, *Am. Chem.* **2011**, *133*, 12881–12898.
[3] M. R. Shaner, H. A. Atwater, N. S. Lewis, E. W. McFarland, *Energy Environ. Sci.* **2016**, *9*, 2354–2371.
[4] G. Centi, E. A. Quadrelli, S. Perathoner, *Energy Environ. Sci.* **2013**, *6*, 1711–1731.
[5] C. F. Shih, T. Zhang, J. Li, C. Bai, *Joule* **2018**, *2*, 1925–1949.
[6] W. Zhou, K. Cheng, J. Kang, C. Zhou, V. Subramanian, Q. Zhang, Y. Wang, *Chem. Soc. Rev.* **2019**, *48*, 3193–3228.
[7] X. Jiang, X. Nie, X. Guo, C. Song, J. G. Chen, *Chem. Rev.* **2020**, *120*, 7984–8034.
[8] J. Zhong, X. Yang, Z. Wu, B. Liang, Y. Huang, *Chem. Soc. Rev.* **2020**, *49*, 1385–1413.
[9] B. B. Asare Bediako, Q. Qian, B. Han, *Acc. Chem. Res.* **2021**, *54*, 2467–2476.
[10] D. Wang, Z. Xie, M. D. Porosoff, J. G. Chen, *Chem.* **2021**, *7*, 2277–2311.
[11] Z. Ma, M. D. Porosoff, *ACS Catal.* **2019**, *9*, 2639–2656.
[12] P. Gao, L. Zhang, S. Li, Z. Zhou, Y. Sun, *ACS Cent. Sci.* **2020**, *6*, 1657–1670.
[13] I. Nezam, W. Zhou, G. S. Gusmao, M. J. Realff, Y. Wang, A. J. Medford, C. W. Jones, *CO2 Util.* **2021**, *45*, 101405.
[14] V. R. Surisetty, A. K. Dalai, J. Kozinski, *Appl. Catal.* **2011**, *404*, 1–11.
[15] J. Pang, M. Zheng, T. Zhang, *Adv. Catal.* **2019**, *64*, 89–191.
[16] F. Zeng, C. Mebrahtu, X. Xi, L. Liao, J. Ren, J. Xie, H. J. Heeres, R. Palkovits, *Appl. Catal. B* **2021**, *291*, 120073.
[17] D. Xu, Y. Wang, M. Ding, X. Hong, G. Liu, S. C. E. Tsang, *Chem.* **2021**, *7*, 849–881.
[18] S. Zhang, Z. Wu, X. Liu, K. Hua, K. Shao, B. Wei, C. Huang, H. Wang, Y. Sun, *Top. Catal.* **2021**, *64*, 371–394.
[19] X. Nie, W. Li, X. Jiang, X. Guo, C. Song, . *Adv. Catal.* **2019**, *65*, 121–233.
[20] H. T. Luk, C. Mondelli, D. C. Ferre, J. A. Stewart, J. Perez-Ramirez, *J. Chem. Soc. Rev.* **2017**, *46*, 1358–1426.
[21] L. Wang, L. Wang, J. Zhang, X. Liu, H. Wang, W. Zhang, Q. Yang, J. Ma, X. Dong, S. J. Yoo, J. G. Kim, X. Meng, F. Xiao, *Angew. Chem. Int. Ed.* **2018**, *57*, 6104–6108.
[22] S. Zhang, X. Liu, Z. Shao, H. Wang, Y. Sun, *J. Catal.* **2020**, *382*, 86–96.
[23] L. Wang, S. He, L. Wang, Y. Lei, X. Meng, F.-S. Xiao, *ACS Catal.* **2019**, *9*, 11335–11340.
[24] Y. Chen, S. Choi, L. T. Thompson, *J. of Catal.* **2016**, *343*,147–56.
[25] C. Yang, R. Mu, G. Wang, J. Song, H. Tian, Z. J. Zhao, J. Gong, *Chem. Sci.* **2019**, *10*, 3161–3167.
[26] H. Kusama, H. Okabe, K. Sayama, H. Arakawa, *Energy* **1997**, *22*, 343–348.
[27] K. K. Bando, K. Soga, K. Kunimori, H. Arakawa, *Appl. Catal. A* **1998**, *175*, 67–81.
[28] F. Zhang, W. Zhou, X. Xiong, Y. Wang, K. Cheng, J. Kang, Y. Wang, *J. Phys. Chem. C* **2021**, *125*(44), 24429–24439.
[29] L. Ding, T. Shi, J. Gu, Y. Cui, Z. Zhang, C. Yang, T. Chen, M. Lin, P. Wang, N. Xue, L. Peng, *Chem.* **2020**, *6*, 2673–2689.
[30] S. Bai, Q. Shao, P. Wang, Q. Dai, X. Wang, X. Huang, *J. Am. Chem. Soc.* **2017**, *139*, 6827–6830.
[31] F. Liao, Y. Huang, J. Ge, W. Zheng, K. Tedsree, P. Collier, X. Hong, S. C. Tsang, *Angew. Chem. Int. Ed.* **2011**, *50*, 2162–2165.
[32] J. Su, Z. Zhang, D. Fu, D. Liu, X. C. Xu, B. Shi, X. Wang, R. Si, Z. Jiang, J. Xu, Y. F. Han, *J. Catal.* **2016**, *336*, 94–106.
[33] S. Kattel, P. J. Ramírez, J. G. Chen, J. A. Rodriguez, P. Liu, *Science* **2017**, *355*, 1296–1299.

[34] F. Goodarzi, L. Kang, F. R. Wang, F. J. Joensen, S. Kegnæs, J. Mielby, *ChemCatChem.* **2018**, *10*, 1566–1570.
[35] J. Mielby, J. O. Abildstrøm, F. Wang, T. Kasama, T. Weidenthaler, C. S. Kegnæs, *Angew. Chem. Int. Ed.* **2014**, *53*, 12513–12516.
[36] A. B. Laursen, K. T. Højholt, L. F. Lundegaard, S. B. Simonsen, S. Helveg, F. Schüth, M. Paul, J. D. Grunwaldt, S. Kegnæs, C. H. Christensen, K. Egebald, *Angew. Chem.* **2010**, *122*, 3582–3585.
[37] R. Pulikkal Thumbayil, J. Mielby, S. Kegnæs, *Top. Catal.* **2019**, *62*, 678–688.
[38] A. Corma, *Chem. Rev.* **1995**, *95*, 559–614.
[39] S. Saravanamurugan, I. Tosi, K. H. Rasmussen, R. E. Jensen, E. Taarning, S. Meier, A. Riisager, *Catal. Sci. Technol.* **2017**, *7*, 2782–2788.
[40] S. Goel, S. I. Zones, E. Iglesia, *J. Am. Chem. Soc.* **2014**, *136*, 15280–15290.
[41] S. Li, A. Tuel, D. Laprune, F. Meunier, D. Farrusseng, *Chem. Mater.* **2015**, *27*, 276–282.
[42] K. H. Rasmussen, F. Goodarzi, D. B. Christensen, J. J. Mielby, S. Kegnæs, *ACS Appl. Nano Mater.* **2019**, *2*, 8083–8091.
[43] K. Miyake, R. Inoue, M. Nakai, Y. Hirota, Y. Uchida, S. Tanaka, M. Miyamoto, N. Nishiyama, *Microporous Mesoporous Mater.* **2018**, *271*, 156–159.
[44] S. Goel, Z. Wu, S. I. Zones, S. E. Iglesia, *J. Am. Chem. Soc.* **2012**, *134*, 17688–17695.
[45] D. Farrusseng, A. Tuel, *New J. Chem.* **2016**, *40*, 3933–3949.
[46] K. T. Højholt, A. B. Laursen, S. Kegnæs, C. H. Christensen, *Top. Catal.* **2011**, *54*, 1026–1033.
[47] C. H. Christensen, K. Johannsen, E. Törnqvist, I. Schmidt, H. Topsøe, C. H. Christensen, *Catal. Today* **2007**, *128*, 117–122.
[48] L. Tosheva, V. P. Valtchev, *Chem. Mater.* **2005**, *17*, 2494–2513.
[49] J. Perez-Ramírez, D. Verboekend, A. Bonilla, S. Abello, *Adv. Funct. Mater.* **2009**, *19*, 3972–3979.
[50] K. Egeblad, C. H. Christensen, M. Kustova, C. H. Christensen, *Chem. Mater.* **2008**, *20*, 946–960.
[51] I. I. Ivanova, E. E. Knyazeva, *Chem. Soc. Rev.* **2013**, *42*, 3671–3688.
[52] J. Abildstrøm, O. Z. N. Ali, U. V. Mentzel, J. Mielby, S. Kegnæs, M. Kegnæs, *New J. Chem.* **2016**, *40*, 4223–4227.
[53] I. I. Ivanova, A. S. Kuznetsov, O. A. Ponomareva, V. V. Yuschenko, E. E. Knyazeva, *Stud. Surf. Sci. Catal.* **2005**, *158*, 121–128.
[54] J. Perez-Ramírez, D. Verboekend, A. Bonilla, S. Abello, *Adv. Funct. Mater.* **2009**, *19*, 3972–3979.
[55] A. H. Janssen, A. J. Koster, K. P. de Jong, *Angew. Chem. Int. Ed.* **2001**, *40*, 1102–1104.
[56] C. Choifeng, B. J. Hall, R. J. Huggins, R. A. Beyerlein, *J. Catal.* **1993**, *140*, 395–405.
[57] F. Liu, T. Willhammar, L. Wang, L. Zhu, Q. Sun, X. Meng, W. Carrillo-Cabrera, X. Zou, F. S. Xiao, *J. Am. Chem. Soc.* **2012**, *134*, 4557–4560.
[58] H. Wang, T. J. Pinnavaia, *Angew. Chem. Int. Ed.* **2006**, *45*, 7603–7606.
[59] I. Schmidt, A. Boisen, E. Gustavsson, K. Ståhl, S. Pehrson, S. Dahl, A. Carlsson, C. J. Jacobsen, *Chem. Mater.* **2001**, *13*, 4416–4418.
[60] C. J. Jacobsen, C. Madsen, J. Houzvicka, I. Schmidt, A. Carlsson, *J. Am. Chem. Soc.* **2000**, *122*, 7116–7117.
[61] S. Han, Z. Wang, L. Meng, N. Jiang, *Mater. Chem. Phys.* **2016**, *177*, 112–117.
[62] Y. Yu, D. Zhang, N. Wei, K. Yang, H. Gong, C. Jin, W. Zhang, S. Huang, *J. Mol. Cat.* **2020**, *483*, 110768.
[63] E. Y. Brazovskaya, O. Y. Golubeva, *Glass Phys. Chem.* **2021**, *47*, 726–730.
[64] M. A. Camblor, A. Mifsud, J. Pérez-Pariente, *Appl. Spectrosc.* **1991**, *11*, 792–797.
[65] X. Zaiku, C. Qingling, Z. Chengfang, B. Jiaqing, C. Yuhua, *J. Phys. Chem.* **2000**, *104*, 2853–2859.
[66] J. M. Newsam, M. M. Treacy, W. T. Koetsier, C. D. Gruyter, *Proc. R. Soc. London Ser. A* **1988**, *420*, 375–405.
[67] K. Egeblad, M. Kustova, S. K. Klitgaard, K. Zhu, C. H. Christensen, *Microporous Mesoporous Mater.* **2007**, *101*, 214–223.
[68] X. Ye, C. Yang, X. Pan, J. Ma, Y. Zhang, Y. Ren, X. Liu, L. Li, Y. Huang, *Crystals. J. Am. Chem. Soc.* **2020**, *142*, 19001–19005.
[69] J. C. Groen, L. A. A. Peffer, J. Pérez-Ramírez, *Microporous Mesoporous Mater.* **2003**, *60*(1-3), 1–17.
[70] J. Graciani, D. C. Grinter, P. J. Ramirez, R. M. Palomino, F. Xu, I. Waluyo, J. A. Rodriguez, *ACS Catal.* **2022**, *12*(24), 15097–15109.
[71] Y. Wang, W. Gao, K. Li, Y. Zheng, Z. Xie, W. Na, H. Wang, *Chem.* **2020**, *6*(2), 419–430.
[72] G. Buntkowsky, M. Vogel, R. Winter, *ZPC* **2018**, *232*, 937–972.
[73] Z. Q. Wang, Z. N. Xu, S. Y. Peng, M. J. Zhang, G. Lu, Q. S. Chen, G. C. Guo, *ACS Catal.* **2015**, *5*(7), 4255–4259.
[74] D. L. Nieskens, D. Ferrari, Y. Liu, Jr., R. Kolonko, *Catal. Commun.* **2011**, *14*, 111–113.
[75] S. Li, H. Guo, C. Luo, H. Zhang, L. Xiong, X. Chen, L. Ma, *Catal.* **2013**, *143*, 345–355.
[76] G. Prieto, S. Beijer, M. L. Smith, M. He, Y. Au, Z. Wang, D. A. Bruce, K. P. De Jong, J. J. Spivey, P. E. De Jongh, *Angew. Chem.* **2014**, *126*, 6515–6519.
[77] Z. He, Q. Qian, J. Ma, Q. Meng, H. Zhou, J. Song, Z. Liu, B. Han, *Angew. Chem.* **2016**, *55*, 737–741.
[78] Y. Lou, F. Jiang, W. Zhu, L. Wang, T. Yao, S. Wang, B. Yang, B. Yang, Y. Zhu, X. Liu, *Appl. Catal.* **2021**, *291*, 120122.
[79] A. Egbebi, V. Schwartz, S. H. Overbury, J. J. Spivey, *Catal. Today* **2010**, *149*, 91–97.
[80] D. Wang, Q. Bi, G. Yin, P. Wang, F. Huang, X. Xie, M. Jiang, *Catal.* **2018**, *148*, 11–22.
[81] K. An, S. Zhang, J. Wang, Q. Liu, Z. Zhang, Y. Liu, *J. Energy Chem.* **2021**, *56*, 486–495.
[82] B. Liu, B. Ouyang, Y. Zhang, K. Lv, Q. Li, Y. Ding, J. Li, *J. Catal.* **2018**, *366*, 91–97.
[83] C. Yang, S. Liu, Y. Wang, J. Song, G. Wang, S. Wang, Z. J. Zhao, R. Mu, J. Gong, *Angew. Chem.* **2019**, *58*, 11364–11369.
[84] D. Xu, M. Ding, X. Hong, G. Liu, S. C. E. Tsang, *Acs Catal.* **2020**, *10*, 5250–5260.
[85] H. Kusama, K. Okabe, K. Sayama, H. Arakawa, *J. Jpn. Pet. Inst.* **1999**, *42*,178–179.
[86] F. J. Caparrós, L. Soler, M. D. Rossell, I. Angurell, L. Piccolo, O. Rossell, J. Llorca, *Chemcatchem.* **2018**, *10*, 2365–2369.
[87] X. Pan, Z. Fan, W. Chen, Y. Ding, H. Luo, X. Bao, *Nat. Mater.* **2007**, *6*, 507–511.
[88] P. Kangvansura, L. M. Chew, W. Saengsui, P. Santawaja, Y. Poo-arporn, M. Muhler, H. Schultz, A. Worayingyong, *Catal.* **2016**, *275*, 59–65.
[89] S. Liu, H. Zhou, Q. Song, Z. Ma, *Taiwan Inst. Chem. Eng.* **2017**, *76*, 18–26.

Manuscript received: June 29, 2023
Revised manuscript received: October 30, 2023
Accepted manuscript online: October 30, 2023
Version of record online: December 5, 2023